Numerical Study of Turbulent Heat Transfer and Pressure Drop Characteristics in a Water-Cooled Minichannel Heat Sink

X. L. Xie

W. Q. Tao
e-mail: wqtao@mail.xjtu.edu.cn

Y. L. He

State Key Laboratory of Multiphase Flow in Power Engineering,
Xi'an Jiaotong University,
Xi'an, Shaanxi 710049, China

With the rapid development of the Information Technology (IT) industry, the heat flux in integrated circuit (IC) chips cooled by air has almost reached its limit at about $100\ \mathrm{W/cm^2}$. *Some applications in high technology industries require heat fluxes well beyond such a limitation. Therefore, the search for a more efficient cooling technology becomes one of the bottleneck problems of the further development of the IT industry. The microchannel flow geometry offers a large surface area of heat transfer and a high convective heat transfer coefficient. However, it has been hard to implement because of its very high pressure head required to pump the coolant fluid through the channels. A normal channel size could not give high heat flux, although the pressure drop is very small. A minichannel can be used in a heat sink with quite a high heat flux and a mild pressure loss. A minichannel heat sink with bottom size of* $20\ \mathrm{mm} \times 20\ \mathrm{mm}$ *is analyzed numerically for the single-phase turbulent flow of water as a coolant through small hydraulic diameters. A constant heat flux boundary condition is assumed. The effect of channel dimensions, channel wall thickness, bottom thickness, and inlet velocity on the pressure drop, temperature difference, and maximum allowable heat flux are presented. The results indicate that a narrow and deep channel with thin bottom thickness and relatively thin channel wall thickness results in improved heat transfer performance with a relatively high but acceptable pressure drop. A nearly optimized structure of heat sink is found that can cool a chip with heat flux of* $350\ \mathrm{W/cm^2}$ *at a pumping power of* 0.314 W. [DOI: 10.1115/1.2753887]

Introduction

With the rapid development of the IT industry, the heat flux in IC chips cooled by air has almost reached its limit at about $100\ \mathrm{W/cm^2}$. Some applications in high technologies require heat fluxes well beyond such a limitation. Therefore, the search for a more efficient cooling technology becomes one of the bottleneck problems of the further development of the IT industry. Microchannel liquid cooling is one of the candidates for this purpose. Microchannel cooling technology was first put forward in 1981 by Tuckerman and Pease [1], who employed the direct water circulation in microchannels fabricated in silicon chips. They were able to reach the highest heat flux of $7.9\ \mathrm{MW/m^2}$ with a maximum temperature difference between substrate and inlet water of 71°C. However, the penalty in pressure drop was also very high; i.e., 200 kPa with plain microchannels and 380 kPa with pin fin enhanced microchannels. Later, Philips [2] analyzed the heat transfer and fluid flow characteristics in microchannels in more detail and provided formulations for designing microchannel geometries. Recently, Kandlikar et al. made a series of studies on the direct liquid cooling technology by microchannels [3–5].

The microchannel flow geometry offers a large surface area of heat transfer and a high convective heat transfer coefficient. However, it has been hard to implement it in a compact/slim design of computers or consumer electronic devices. The major difficulty is driving water with high pressure head, which is required to pump the coolant fluid though the channels. A normal channel could not give such high heat flux, although the pressure drop is very low. Thus, an idea comes into being that a water-cooled minichannel can be used in a heat sink with a high heat flux and a mild pressure loss. Here, by minichannels, we refer to the channels with their characteristic lengths within 0.2–3 mm [6]. In the following, a brief review on fluid flow and heat transfer of liquids in minichannels is presented.

Convective heat transfer and fluid flow in a minichannel and their application in the cooling technology of electronic devices has attracted great attention of researchers in recent years. Reference [7] indicated that the heat conduction in the walls of mini/microchannels makes the heat transfer multidimensional, and the axial conduction in the walls cannot be neglected. The surface roughness effects on pressure drop in single-phase flow in minichannels were investigated in Refs. [6,8–11]. Gao et al. [12] made experimental investigations of scale effects on hydrodynamics and the associated heat transfer in two-dimensional mini- and microchannels with channel height ranging from 0.1 mm to 1 mm. Their results showed that the conventional laws of hydrodynamics and heat transfer can be applied for channels with height larger than 0.4 mm. Reference [13] experimentally examined the frictional characteristics inside minichannels ($D_h = 0.198-2.01$ mm) with water and lubricant oil as the working fluids, and the tests were performed in both round and rectangular configurations. The test results indicated a negligible influence of viscosity on the friction factor if the hydraulic diameter is greater than 1.0 mm, and the measured data can be well predicted by the conventional correlation in both laminar and turbulent flow conditions. Reference [14] presented an experimental study of friction factor and heat transfer coefficient for a vertical liquid upflow of R-134a in minichannels. References [15,16] experimentally investigated the single- and two-phase flow pressure drop and heat transfer characteristics in straight and miniature helical flow passages with R-134a as a working fluid. Measurement of forced

Contributed by the Electrical and Electronic Packaging Division of ASME for publication in the JOURNAL OF ELECTRONIC PACKAGING. Manuscript received November 29, 2005; final manuscript received December 13, 2006. Review conducted by Andrew Y.-H. Hung.

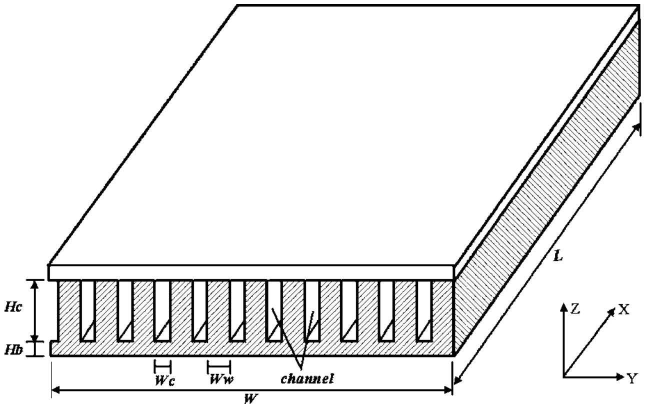

Fig. 1 Schematic view of a minichannel geometry for high heat flux cooling applications

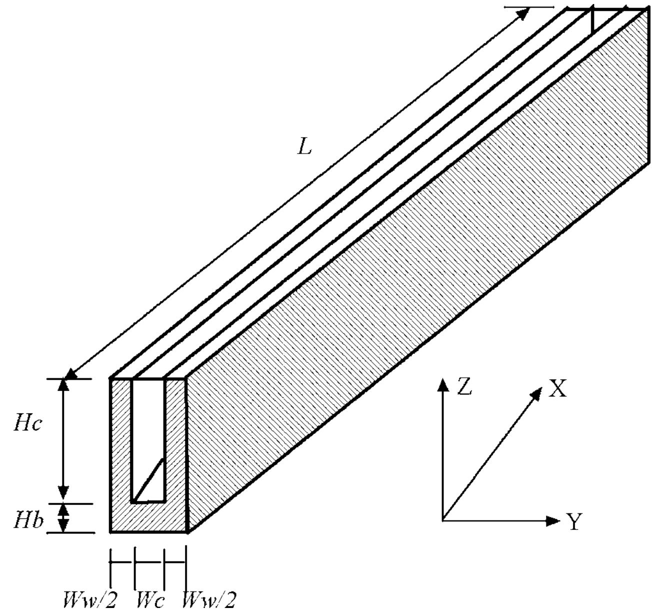

Fig. 2 Computational domain for minichannel

convection heat transfer coefficients in minichannels was performed in Ref. [17]. Reference [18] measured the friction and heat transfer coefficients in 2D minichannels of 1.12 mm to 0.3 mm in thickness, and experimental results are in good agreement with classical correlations relative to channels of conventional size. From all the above-mentioned references, the following conclusions can be drawn: (1) In the liquid minichannels, the conventional physical and mathematical models for fluid flow and heat transfer with no-slip boundary conditions are still valid; (2) The friction factor and heat transfer correlations for conventional channels can also be used in minichannels as long as their relative surface roughness and relative wall thickness are not too high. The use of minichannels in the cooling technology of electronic devices can be found in the following references. In Ref. [19], a microprocessor package with water cooling was proposed in which a narrow water jacket was used to cool a thermal spread attached to the silicon die backside for an efficient cooling. Schmidt [20] described a microprocessor liquid cooled minichannel heat sink and presented its performance as applied to a microprocessor (IBM Power 4) chip. In Ref. [21], an analytical model for laminar flow was given and a numerical study was conducted for the channel optimization in a cooling spreader on a smaller and transient heat source. It was concluded that when small pumping power was available, a deeper channel with a thicker base was the best profile for the miniature channel coolers, and the best cooling performance was found at 0.0586 K/W for 0.03 W pumping power.

The aim of this study is to numerically design a water-cooling jacket that has relatively high heat transfer performance while keeping the pressure drop in an acceptable range. In the present paper, a multi-minichannel device has been designed and three-dimensional numerical simulations for its heat transfer and friction characteristics have been performed. In the following, the outlines of such a jacket will first be introduced and followed by its physical and mathematical models. Next, 3D computational results will be presented along with performance comparisons. Finally, some conclusions will be drawn.

Description of the Designed Cooling Model

Figure 1 shows a pictorial view of the suggested model. The unvaried total area being cooled is $W \times L$ with individual minichannel flow passage dimensions of $W_c \times H_c$. The wall separating the two channels is of thickness W_w and acts like a fin. The bottom thickness is H_b. The top cover is bonded, glued, or clamped to provide closed channels for liquid flow.

The channel dimensions W_c and H_c, the fin thickness W_w, bottom thickness H_b, and the coolant flow velocity U_{in} are the parameters of interest in designing a minichannel heat sink. Their effects on thermal performance and pressure drop are examined in this paper. The maximum allowable temperature of the bottom surface, the minimum coolant inlet temperature, and the acceptable pressure drop are the constraints. In addition, there are manufacturing and cost constraints that need to be considered in any practical system design. However, in the following discussion, the manufacturing and cost constraints are not taken into account.

Mathematical Formulation and Numerical Methods

To analyze the thermal and flow characteristics of this model, the following assumptions are made:

(1) The flow is three dimensional, incompressible, turbulent, and in steady state.
(2) The effect of body force is neglected.
(3) The fluid thermophysical properties are constant and heat dissipation is neglected.
(4) All minichannels are supposed to be identical in heat transfer and fluid flow; hence, one channel can be picked out as the representation for computation as shown in Fig. 2, where the coordinate system is indicated.

The governing equations along with the standard k-ε turbulence model based on the above assumptions are as follows.

Conservation of mass:

$$\frac{\partial}{\partial x_i}(\rho u_i) = 0 \tag{1}$$

Conservation of momentum:

$$\frac{\partial}{\partial x_i}(\rho u_i u_j) = -\frac{\partial p}{\partial x_j} + \frac{\partial}{\partial x_i}\left[(\mu+\mu_t)\frac{\partial u_j}{\partial x_i}\right] + \frac{\partial}{\partial x_i}\left[(\mu+\mu_t)\frac{\partial u_i}{\partial x_j}\right], \quad j = 1,2,3 \tag{2}$$

Conservation of energy:

$$\frac{\partial}{\partial x_i}(\rho u_i T) = \frac{\partial}{\partial x_i}\left[\left(\frac{\lambda}{c_p} + \frac{\mu_t}{\sigma_T}\right)\frac{\partial T}{\partial x_i}\right] \tag{3}$$

Conservation of turbulence kinetic energy:

$$\frac{\partial}{\partial x_i}(\rho k u_i) = \frac{\partial}{\partial x_i}\left[\left(\mu + \frac{\mu_t}{\sigma_k}\right)\frac{\partial k}{\partial x_i}\right] + G_k - \rho\varepsilon \tag{4}$$

Conservation of turbulence dissipation rate:

$$\frac{\partial}{\partial x_i}(\rho \varepsilon u_i) = \frac{\partial}{\partial x_i}\left[\left(\mu + \frac{\mu_t}{\sigma_\varepsilon}\right)\frac{\partial \varepsilon}{\partial x_i}\right] + \frac{\varepsilon}{k}(c_1 G_k - c_2 \rho \varepsilon) \quad (5)$$

where k and ε are turbulence kinetic energy and turbulence dissipation rate, respectively, and G_k represents the generation of turbulence kinetic energy, which can be expressed as

$$G_k = -\rho \overline{u_i' u_j'} \frac{\partial u_j}{\partial x_i} \quad (6)$$

The turbulent viscosity μ_t is defined as

$$\mu_t = \rho C_\mu k^2/\varepsilon \quad (7)$$

where C_μ=0.09, C_1=1.44, C_2=1.92, σ_k=1.0, σ_ε=1.3, and σ_T=0.9.

In order to facilitate the investigation of channel geometry effects and the channel thermal conductivity effect, the numerical simulation was conducted for the entire computational domain, with the solid region being treated as a special liquid. This implies that the computation is of conjugated type [22,23]. The no-slip hydraulic boundary condition of velocity is adopted for the solid wall, the inlet distribution is uniform for velocity at the channel inlet, and the outlet boundary condition is considered of local one-way type [22,23]:

$$x=0 \quad u=U_{\text{in}} \quad v=w=0 \quad (8)$$

$x=L$ the influence coefficient of the downstream equals zero (9)

$$u=0 \quad v=0 \quad w=0 \quad \text{at solid walls} \quad (10)$$

The velocities in the solid region are zero everywhere, which is automatically guaranteed by a numerical solution algorithm for the conjugated problem [22,23].

The thermal boundary conditions are given as follows. The left and right surfaces are the symmetry planes, and the boundary conditions are adiabatic:

$$y=0 \quad \frac{\partial T}{\partial y}=0 \quad (11)$$

$$y=W_c+W_w \quad \frac{\partial T}{\partial y}=0 \quad (12)$$

At the bottom position, the heat flux is given:

$$z=0 \quad -\lambda_s \frac{\partial T}{\partial z}=q_w \quad (13)$$

The top surface is assumed to be adiabatic:

$$z=H_b+H_c \quad -\lambda_s \frac{\partial T}{\partial z}=0 \ \text{(for solid)} \quad -\lambda_f \frac{\partial T}{\partial z}=0 \ \text{(for liquid)} \quad (14)$$

At the inlet position, the inlet temperature of liquid is given to be constant, and the outlet boundary is considered of local one-way type [22,23]:

$$x=0 \quad T=T_{\text{in}} \quad (15)$$

$x=L$ the influence coefficient of the downstream equals zero (16)

The wall function approach [23] is adopted to model the near-wall region. For k and ε, the local one-way type boundary condition [22,23] is used at the outlet and the Neumann condition is adopted on the symmetry boundary.

The discretization of the governing equations in the computational domain is performed on a staggered grid by using the finite volume approach. A stability-guaranteed second-order difference scheme [24] is used to discretize the convective terms, while the others are approximated by the center-difference approach. The SIMPLE solution algorithm is adopted to deal with the linkage between pressure and velocities, the details of which can be found in Refs. [22,23]. It should be noted that the problem at hand is a conjugated one, in that both the fluid temperature and the temperatures in the channel walls are to be simultaneously determined during the computation. For this purpose, the harmonic mean method was used to determine the diffusion coefficient at the control volume interface [22,23], and to keep the heat flux continuum at the interface, the thermal conductivity at the different material regions adopted individual values while the heat capacity of fluid was used for all the fluid and solid regions, because the nominal diffusion coefficient in the energy equation is λ/c_p, rather than λ itself. The deferred correction [23] is applied to deal with the high-order difference scheme for the convective term. Each of the discretized equations then forms a tridiagonal matrix, which can be solved by the alternative direction iteration (ADI) with ease [22,23].

Table 1 Range of test parameters

U_{in} (m/s)	2	3	4	5	6		
W_c (mm)	0.5	0.6	0.7	0.8			
H_c (mm)	2	3	4	5	6		
W_w (mm)	0.1	0.2	0.3	0.4	0.6	0.8	1.0
H_b (mm)	0.1	0.2	0.3	0.5	0.7	0.9	

It is well known that the channel width and the channel aspect ratio (H_c/W_c) have significant effects on the performance of a minichannel heat sink. In order to get a better thermal performance and acceptable mild pressure drop, the effects of the channel geometry and inlet velocity are investigated parametrically, and the range of the geometric parameters and the inlet velocity are shown in Table 1. The width of channel from 0.5 to 1.0 mm can be easily manufactured with current conventional fabrication technology, and H_c should not be very large for the consideration of compactness and ease of manufacturing. The hydraulic diameter D_h of the fluid flow channel and Reynolds number Re are defined, respectively, as

$$D_h = \frac{4W_c H_c}{2(W_c+H_c)} \quad (17)$$

$$\text{Re} = \frac{U_m D_h}{\nu} \quad (18)$$

where U_m is the mean fluid velocity in a minichannel, which is equal to inlet velocity U_{in}, and ν is the kinematic viscosity of fluid. When the Re is larger than 2300, the flow regime in the minichannel is considered turbulent. All the Reynolds numbers are larger than 2300 with the parameters listed in Table 1 and the kinematic viscosity of water at 35°C in the following calculation. The inlet temperature of the water is 300 K. The thermophysical properties of water at 35°C are used in the numerical simulation. The material of heat sink is pure copper. The bottom dimension is 20 mm×20 mm, which was determined according to the conventional chip sizes. Since the channel width spans quite a large variation, the grid systems are different for individual cases. After a grid independence examination, the grid system used in the present model is at least 200×30×80 in the x-, y-, and z-axes, which is for the case with bottom thickness of 0.1 mm and channel vertical wall thickness of 0.3 mm. The finest grid system adopted in the computation has nodes as large as 840,000. The grid independent examination is illustrated in Fig. 3, where the temperature difference between bottom maximum temperature and fluid inlet temperature is displayed. The parameters are W_c=0.5 mm, H_c=5 mm, W_w=0.3 mm, H_b=0.3 mm, and U_{in}

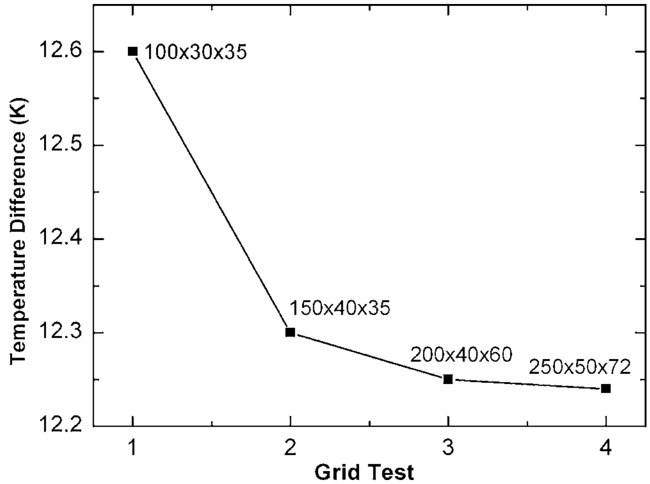

Fig. 3 Grid test for minichannel with W_c=0.5 mm, H_c=5 mm, W_w=0.3 mm, H_b=0.3 mm, and U_{in}=3 m/s

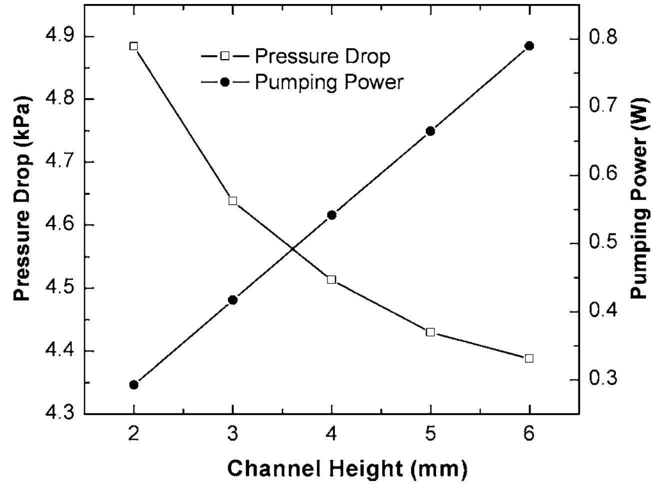

Fig. 4 Effect of channel height on pressure drop and pumping power

=3 m/s, respectively. The deviation between case 3 (200×40×60) and case 4 (250×50×72) is very small (far less than 1%), so the grid system of case 3 is adopted for the parameter combination mentioned above.

If the relative deviation between two consecutive iterations is less than the specified small value ε_ϕ, the iteration is considered converged

$$\max(|\phi^n_{i,j,k}-\phi^{n-1}_{i,j,k}|/|\phi^n_{i,j,k}|) < \varepsilon_\phi \tag{19}$$

where ϕ represents the variables u,v,w,t,k, and ε. $\varepsilon_\phi=10^{-7}$ is used in this paper.

Results and Discussion

Definition of overall thermal resistance θ is

$$\theta=\frac{T_{\max}-T_{\text{in}}}{Q} \tag{20}$$

$$Q=qA_b \tag{21}$$

where $T_{\max}$ is the maximum bottom temperature, T_{in} is the inlet fluid temperature, Q is the total heat generation, q is the bottom heat flux, and A_b is the whole heating area of the heat sink.

Supplied pumping power W_{pp} to generate the flow is defined in Eq. (22) as

$$W_{\text{pp}}=\dot{V}\Delta p \tag{22}$$

where $\dot{V}$ is the volumetric flow rate, and Δp is the pressure drop through the heat sink.

The effects of channel width W_c, channel height H_c, bottom thickness H_b, vertical wall thickness W_w, and inlet velocity U_{in} are studied parametrically. The numerical results will first be presented about the influences of those parameters on the water pressure drop Δp through the cooling device and the thermal resistance θ in the device. When the pressure drop Δp and thermal resistance θ are studied, the bottom heat flux q_w is assumed to be 100 W/cm^2, while when the effect on the maximum heat flux $q_{\max}$ is concerned, the maximum temperature difference ΔT is taken as 50°C. Attention is then turned to seek the nearly optimum configuration of the minichannel, and the corresponding geometries are proposed. Finally, some conclusions are drawn.

In the parametric study, only one parameter is varied while all the others are kept constant, and the values of other parameters are initiated at first. After the effect of a parameter has been investigated and a best value of the parameter has been obtained with other parameters remaining constant, the best value found in such a way is assumed to be the best value for all other parameter combinations, and is used in the successive study for other parameters.

Effect of Channel Height. The relations of the pressure drop and pumping power with channel height are shown in Fig. 4. The computations were conducted for the case of inlet velocity of 3 m/s, bottom thickness of 1 mm, and channel wall thickness and channel width of 0.5 mm.

As shown in Fig. 4, the pressure drop decreases with the increase in channel height. The flow rate per channel increases linearly with an increase in channel height at constant inlet velocity, while the corresponding pressure loss decreases mildly. As can be observed in the figure, the pressure drop has about a 10% decrease from channel height of 2 mm to 6 mm. The pumping power increases with channel height, and the slope of the pumping power versus channel height shows a linear variation.

Figure 5 shows that the variation of the thermal resistance with channel height has a trend similar to the pressure drop versus channel height. It can be observed from the figure that for the case studied, a further increase in the channel height makes no contribution to the increase of the maximum heat flux. The maximum

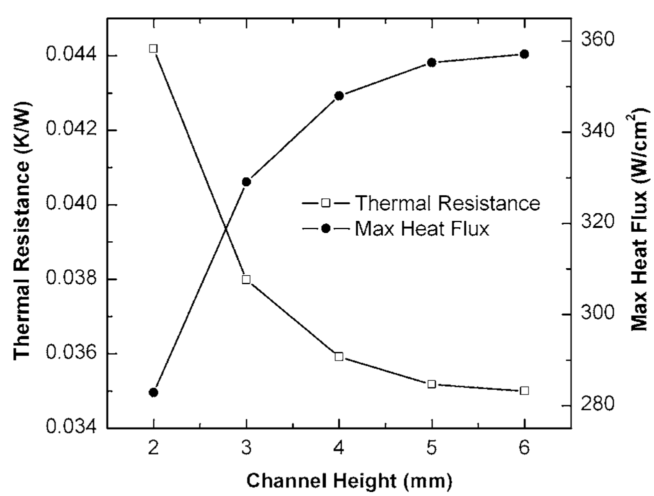

Fig. 5 Effect of channel height on thermal resistance and max heat flux

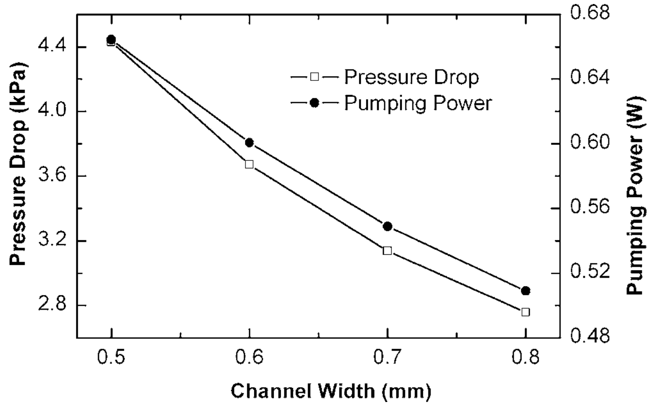

Fig. 6 Effect of channel width on pressure drop and pumping power

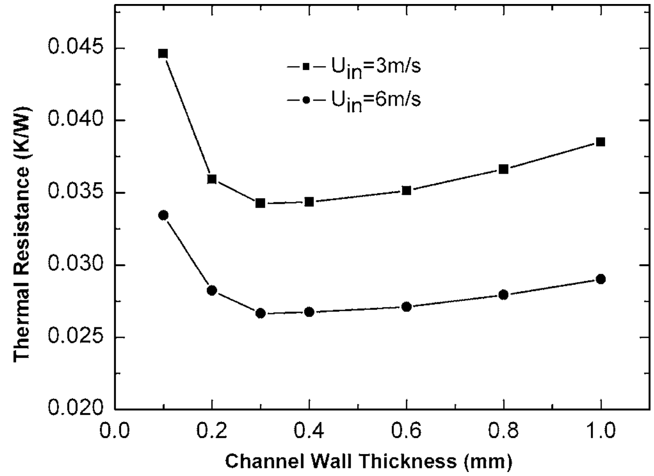

Fig. 8 Effect of channel wall thickness on thermal resistance

heat flux deviation is less than 1% for channel heights of 5 mm and 6 mm. Thus, in the following discussion, a channel height of 5 mm will be chosen as the optimal value.

Effect of Channel Width. When the effect of channel width is considered, the channel height is fixed at 5 mm with other geometry remaining the same as for the above case. An additional constraint of temperature difference 50 K is applied to study the variation of maximum heat flux with channel width. The variations of pressure drop and pumping power with channel width are shown in Fig. 6. They both have the same variation trend and both decrease with the increase of channel width. Maximum heat flux also decreases with the channel height, while the thermal resistance varies in the opposite direction, as shown in Fig. 7. From the variation of thermal resistance with channel dimensions shown in Figs. 5 and 7, it is found that a narrow and deep channel is better for heat transfer, in spite of a higher pressure drop penalty. To keep a reasonable balance between pressure drop and heat flux, the channel width of 0.5 mm will be chosen as the optimal value in the following discussion.

Effect of Channel Vertical Wall Thickness. Figure 8 represents the variation trend of thermal resistance versus channel vertical wall thickness. The computations are conducted for the case of inlet velocity of 3 m/s and 6 m/s, channel height of 5 mm, channel width of 0.5 mm, and bottom thickness of 1 mm. Simulation results show that the vertical wall thickness has a more significant effect on the thermal resistance, and there is a turning point of wall thickness at which the thermal resistance reaches its minimum. This variation pattern can be analyzed as follows. The heat transfer process from the bottom to the cooling water of the channel includes two thermal resistances in series: the conductive thermal resistance through the vertical wall, and the convective thermal resistance of the side wall, which is fixed at the given inlet velocity and the given side wall surface area. When the vertical wall thickness W_w is too narrow, the conductive thermal resistance predominated and the increase in W_w reduced the conductive thermal resistance, and hence, the total thermal resistance. However, a further increase in W_w leads to a significant increase in the total heat transfer rate entering the computational unit for the fixed heat flux condition, and this causes the increase in $T_{\max}$ in order to transfer the increased total heat transfer rate at the fixed convective heat transfer condition. The turning point at the wall thickness of 0.3 mm appears the same for the inlet velocities of 3 m/s and 6 m/s. Thus, it is considered that the thickness of 0.3 mm is the optimum one of the vertical walls for the inlet velocity range studied.

Effect of Bottom Plate Thickness. Figure 9 shows the effect of bottom plate thickness on thermal resistance. The computations are conducted for the case of inlet velocities of 3 m/s and 6 m/s, channel height of 5 mm, channel wall thickness of 0.3 mm, and channel width of 0.5 mm. Pressure drop and pumping power remained unchanged for each inlet velocity due to the fixed channel

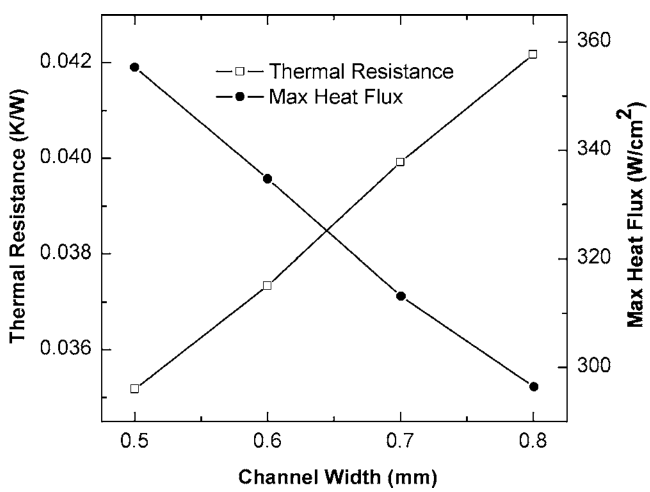

Fig. 7 Effect of channel width on thermal resistance and max heat flux

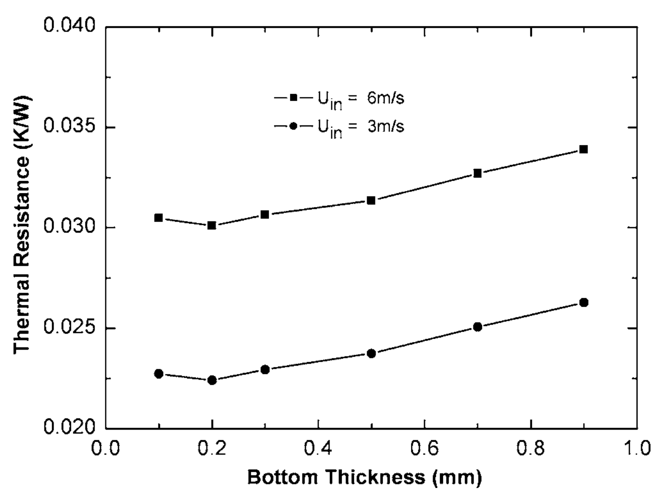

Fig. 9 Effect of bottom thickness on thermal resistance

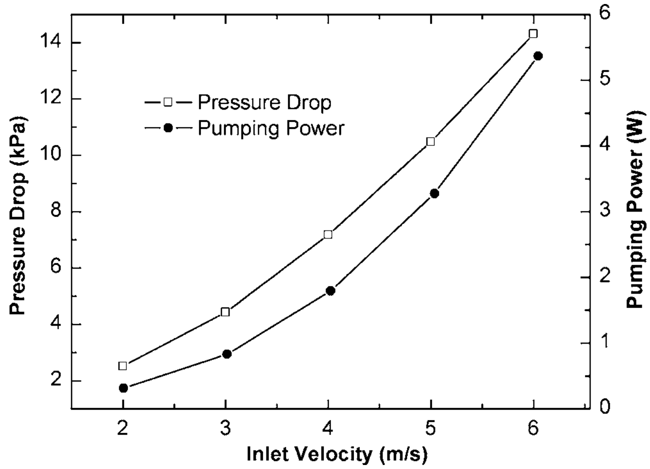

Fig. 10 Pressure drop and pumping power by inlet velocity based on nearly optimal channel geometry

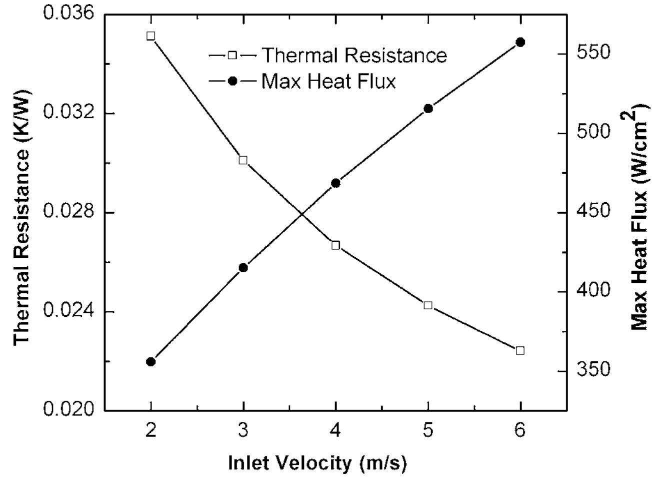

Fig. 11 Thermal resistance and maximum heat flux by inlet velocity based on nearly optimal channel geometry

dimensions. From the figure, it can be seen that the thermal resistance first decreases with the increase of bottom plate thickness, reaches its minimum at 0.2 mm, and then increases with the increase in the thickness. The variation trends are the same for the two inlet velocities of 6 m/s and 3 m/s. The heat transfer rate entering into the bottom surface of H_b is transferred through two ways: One way is the conduction from the bottom surface to the top surface of H_b and the other is from the bottom surface to the two side walls of the computational unit. The first part increases with the decrease of H_b, while the second part decreases with the decrease of H_b. The above-mentioned variation trend results from the balancing between the heat conduction of the two parts. In the following discussion, the bottom thickness of 0.2 mm will be chosen as the optimal value.

Effect of Inlet Velocity. From the above discussion about the influences of parameters of interest on the pressure drop and thermal resistance, we can obtain a nearly optimized structure of the heat sink as follows: W_c=0.5 mm, H_c=5 mm, H_b=0.2 mm, and W_w=0.3 mm. By nearly optimized we mean the fact that the above structure is obtained through simulations that do not cover all the parameter combinations, because the number of all parameter combinations, including inlet velocity, achieves several thousand. For this nearly optimized structure, there are a total of 25 channels for the fixed width of the heat sink.

Simulations of the inlet velocity effect were conducted for this nearly optimized structure, and the results are presented in Figs. 10–12. The effect of inlet velocity on pressure drop and pumping power at the constraint of a temperature difference of 50 K is shown in Fig. 10. Pressure loss varies from about 2500 Pa at an inlet velocity of 2 m/s to about 14,300 Pa at an inlet velocity of 6 m/s, while pumping power varies from 0.314 W to 5.365 W. The variations of thermal resistance and maximum heat flux with inlet velocity are shown in Fig. 11. Thermal resistance decreases with the inlet velocity, while the maximum heat flux increases. The thermal resistance decreases with the increase of inlet velocity, and its slope decreases gradually. This is because the increase in inlet velocity can reduce the convective thermal resistance, which is only a part of the total thermal resistance. With the decrease in the convective thermal resistance, the conductive part becomes more and more important, and this leads to a lesser effect of the reduction in the convective thermal resistance. Therefore, at relatively high inlet velocity, the gain in the total thermal resistance reduction is obtained with a high penalty of pressure drop. The thermal resistance is 0.0224 K/W and the maximum heat flux is 557.6 W/cm^2 at an inlet velocity of 6 m/s. At the low inlet velocity of 2 m/s, the thermal resistance and the maximum heat flux are 0.035 K/W and 350 W/cm^2, respectively. For this nearly optimized structure, the relationship between thermal resistance and pumping power under the above conditions is presented in Fig. 12.

Figure 13 presents the temperature contour at the outlet of channel for the nearly optimized structure at the bottom heat flux of 100 W/cm^2 and inlet velocity of 2 m/s. It can be clearly observed that in most parts of the cooling water, the temperature almost has no change and is still equal to the inlet value of 300 K. The water temperature varies sharply only in the thin layer adjacent to the vertical walls. For the case studied, the thickness of this thin layer, or thermal boundary layer, is about 0.1 mm. That means a microchannel with a width of 200 μm can effectively cool the surface, because all the water in the channel can fully take part in the convective heat transfer. This is the reason that a microchannel has such high effectiveness for electronic cooling. The only drawback of the microchannel cooling device is its very high pressure drop. This drawback motivated the present study.

Comparison With Correlations. As mentioned in the Introduction, conventional correlations can be used to predict the pressure drop and heat transfer in minichannels. Thus, pressure drop Δp can be obtained through the conventional Darcy friction factor f according to the Filonenko correlation [25]

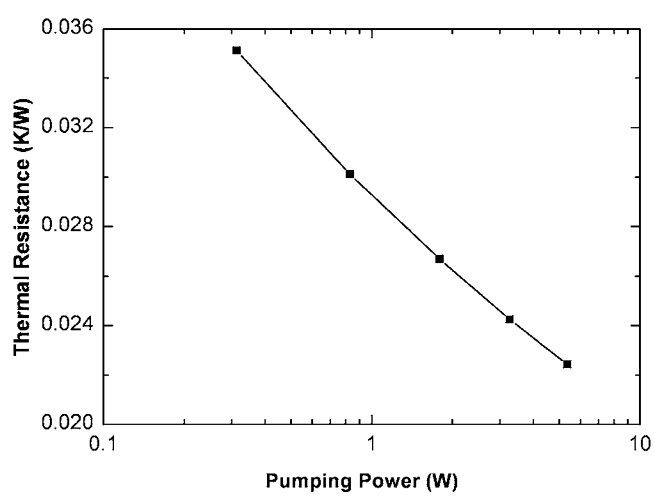

Fig. 12 Thermal resistance by pumping power based on nearly optimal channel geometry

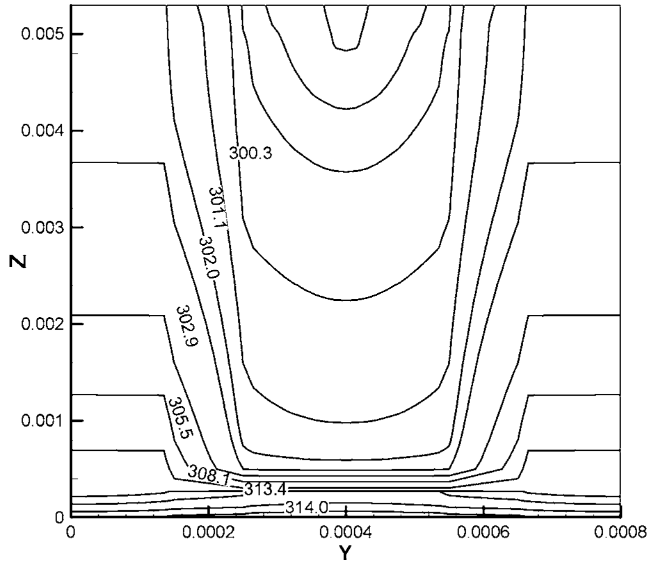

Fig. 13 Temperature contour at outlet with heat flux 100 W/cm^2 and inlet velocity of 2 m/s (unit=m)

$$f = (1.82 \lg \mathrm{Re} - 1.64)^{-2} \tag{23}$$

$$\Delta p = f \frac{L}{D_h} \frac{\rho U_m^2}{2} \tag{24}$$

For the determination of the Nusselt number Nu, we use the classical Colburn correlation [26]

$$\mathrm{Nu} = 0.023\, \mathrm{Re}^{0.8}\, \mathrm{Pr}^{1/3} \tag{25}$$

where the Reynolds number is defined in Eq. (18) and Pr is the Prandtl number of the fluid.

The convective heat transfer coefficient h can be obtained from the Nusselt number

$$h = \frac{\mathrm{Nu}\, \lambda_f}{D_h} \tag{26}$$

where D_h is the hydraulic diameter and λ_f is the thermal conductivity of the fluid.

The heat sink can be analyzed as a two-dimensional flow through narrow rectangular channels with a constant heat flux boundary condition at the base of the fins; capacity resistance and convective resistance were considered in Ref. [27]. Here, conductive resistance is also included when the thickness of the bottom is taken into account. Thermal resistance θ, including three thermal resistance terms, is expressed by

$$\theta = \frac{1}{hA_{\mathrm{sf}}} + \frac{1}{\dot{m} c_p} + \frac{1}{\lambda_s A_b / H_b} \tag{27}$$

where $\dot{m}$ is the total mass flow rate of coolant through channels and A_b is the bottom area. The inclusion of the capacity resistance comes from the fact that the definition of the total thermal resistance θ is based on the temperature difference of $(T_{\max} - T_{\mathrm{in}})$ (see Eq. (20)).

The surface area available for heat transfer (A_{sf}) can be written as [28]:

$$A_{\mathrm{sf}} = nW_c L + 2n\eta H_c L \tag{28}$$

where n is the number of cooling channels and the fin efficiency η is expressed as:

$$\eta = \frac{\tanh(mHc)}{mHc} \tag{29}$$

where W_c is the width of the channels and m is defined as

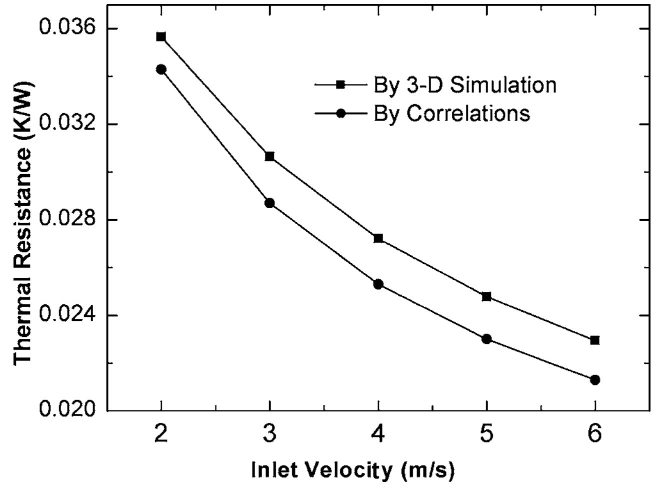

Fig. 14 Results: Comparison on the effect of inlet velocity on thermal resistance

$$m = \sqrt{\frac{2h}{\lambda_s W w}} \tag{30}$$

for the assumption that $L \gg W_b$.

Comparison calculations were performed between the 3D numerical simulation and correlation approach, as mentioned above. Figures 14 and 15 display the effect of inlet velocity on thermal resistance and pressure drop for a nearly-optimized structure based on the two methods, respectively. The two curves of thermal resistance shown in Fig. 14 are in good agreement with each other with a maximum difference of about 8%. Pressure drop profiles also match each other quite well and the maximum deviation is less than 5%, with inlet flow velocity from 3 m/s to 6 m/s while the maximum deviation is about 16.5% at 2 m/s. The reason for this relatively large deviation may be because the Reynolds number at 2 m/s is located nearby the transition region, and the conventional correlations are valid for the fully developed region. In conclusion, results of the 3D numerical simulation coincide with that of the conventional correlation approach quite well. It should be emphasized that the quite good agreement does not necessarily mean that the 3D numerical simulation is not useful, rather, it is the 3D numerical simulation that can account for the complicated effects of different factors and gives a clear physical understanding of the heat transfer and fluid flow process. Only

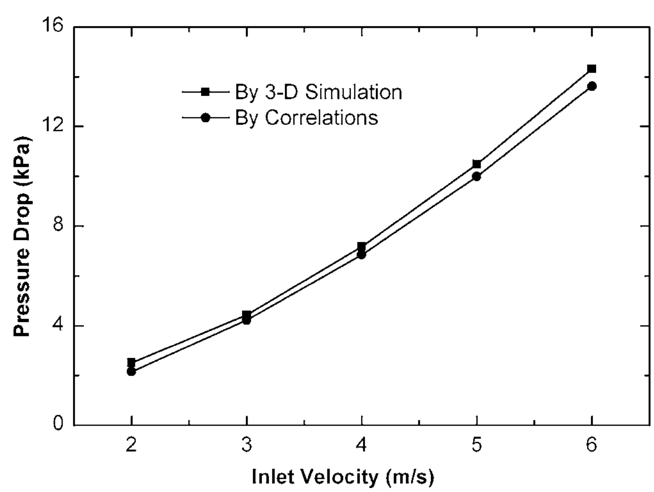

Fig. 15 Results: Comparison on the effect of inlet velocity on pressure drop

when the comparison between the prediction of the 3D simulation and the correlation prediction ensures their agreement can the correlation method then be used in the preliminary design of the cooling devices.

Conclusions

The heat transfer and pressure drop characteristics for single-phase turbulent flow in minichannel heat sinks are analyzed in the present paper. The results are presented for a chip with an active cooling area of 20 mm$\times$20 mm. Comparison was performed and showed that for the cases studied, the results of conventional correlations are in quite good agreement with that of 3D simulations. From the results and analysis, the following conclusions can be obtained:

(1) Pressure drop, an important parameter for minichannel heat sink design, is a strong function of the channel geometry. With respect to heat transfer, a narrow and deep channel is better than that of a wide and shallow channel, in spite of the higher pressure drop penalty. To keep a reasonable balance between pressure drop and heat flux, an optimized study should be conducted for every given case.
(2) Both channel vertical wall thickness and bottom plate thickness have an optimum value at which thermal resistance reaches its minimum.
(3) A nearly optimized configuration is obtained for the heat sink with a bottom size of 20 mm$\times$20 mm. For this heat sink, the maximum heat flux reaches about 557 $\mathrm{W/cm^2}$ under the constraint of temperature difference 50 K with inlet velocity of 6 m/s; the corresponding thermal resistance is 0.0224 K/W and pumping power is 5.365 W. Even at lower inlet velocity of 2 m/s, the thermal performance is also quite good with thermal resistance of 0.035 K/W, pumping power of 0.314 W, and the maximum heat flux of 350 $\mathrm{W/cm^2}$.

Acknowledgment

This work has been supported by the National Natural Science Foundation of China (Grant Nos. 50476046 and 50425620).

Nomenclature

A = area ($\mathrm{m^2}$)
c_p = specific heat capacity (J/Kg K)
D_h = hydraulic diameter of the fluid flow channel (m)
f = friction factor
H = height or thickness (m)
h = heat transfer coefficient ($\mathrm{W/m^2\,K}$)
L = channel length (m)
$\dot{m}$ = total mass flow rate of coolant through channels (kg/s)
Nu = Nusselt number
n = number of cooling channels
p = pressure (Pa)
Δp = pressure drop (Pa)
Q = heat generation (W)
q = heat flux ($\mathrm{W/m^2}$)
T = temperature (K)
Re = Reynolds number
u,v,w = velocity of x,y,z, respectively (m/s)
U_{in} = inlet velocity (m/s)
$\dot{V}$ = volumetric flow rate ($\mathrm{m^3/s}$)
W = width of heat sink (m)
W_{pp} = pumping power (W)
k = turbulence kinetic energy ($\mathrm{m^2/s^2}$)

Greek Symbols

ρ = density ($\mathrm{kg/m^3}$)
μ = dynamic viscosity (kg/m s)
λ = thermal conductivity (W/m K)
η = fin efficiency
σ = Prandtl number
ε = turbulence dissipation rate ($\mathrm{m^2/s^3}$)
υ = kinematic viscosity of fluid ($\mathrm{m^2/s}$)
ϕ = general variable
θ = thermal resistance (K/W)

Subscripts

b = bottom
c = channel
f = fluid
in = inlet
max = maximum value
s = solid
sf = surface available for heat transfer
t = turbulent
w = wall

References

[1] Tuckerman, D. B., and Pease, R. F. W., 1981, "High Performance Heat Sink for VLST," IEEE Electron Device Lett., **EDL-2**(5), pp. 126–129.
[2] Philips, R. J., 1987, "Forced Convection, Liquid Cooled, Microchannel Heat Sinks," MS thesis, Department of Mechanical Engineering, Massachusetts Institute of Technology, Cambridge, MA.
[3] Kandlikar, S. G., and Upadhye, H. R., 2004, "Optimization of Microchannel Geometry for Direct Chip Cooling Using Single Phase Transfer," *Proceedings of Microchannels and Minichannels-2004*, ASME, New York, pp. 679–685.
[4] Kandlikar, S. G., and Grande, W. J., 2004, "Evaluation of Single Phase Flow in Microchannels for High Flux CHIP Cooling—Thermohydraulic Performance Enhancement and Fabrication Technology," *Proceedings of Microchannels and Minichannels-2004*, ASME, New York, pp. 67–76.
[5] Kandlikar, S. G., 2005, "High Flux Heat Removal With Microchannels—A Roadmap of Challenges and Opportunities," *Proceedings of Microchannels and Minichannels-2005*, ASME, Toronto, pp. 1–10.
[6] Kandlikar, S. G., Schmitt, D., Carrano, A. L., and Taylor, J. B., 2005, "Characterization of Surface Roughness Effects on Pressure Drop in Single-Phase Flow in Minichannels," Phys. Fluids, **17**(10) p. 100606.
[7] Gael, M., Isabelle, P., and Denis, M., 2004, "Mini- and Micro-channels: Influence of Axial Conduction in the Walls," Int. J. Heat Mass Transfer, **47**, pp. 3993–4004.
[8] Schmitt, D. J., 2004, "Experimental Investigation of Surface Roughness Microstructures and Their Effects on Pressure Drop Characteristics in Rectangular Minichannels," MS thesis, Department of Mechanical Engineering, Rochester Institute of Technology, Rochester, NY.
[9] Schmitt, D. J., and Kandlikar, S. G., 2004, "Effects of Repeating Microstructures on Pressure in Rectangular Minichannels," *Third International Conference on Microchannels and Minichannels*, Toronto, Canada, June 13–15.
[10] Guo, Z. Y., and Li, Z. X., 2003, "Size Effect on Microscale Single-Phase Flow and Heat Transfer," Int. J. Heat Mass Transfer, **46**, pp. 149–159.
[11] Li, Z., He, Y. L., Tang, G. H., and Tao, W. Q., 2007, "Experimental and Numerical Studies of Liquid Flow and Heat Transfer in Microtubes," Int. J. Heat Mass Transfer, **50**, pp. 3447–3460.
[12] Gao, P. Z., Person, S. L., and Favre-Marinet, M., 2002, "Scale Effects on Hydrodynamics and Heat Transfer in Two-Dimensional Mini and Microchannels," Int. J. Therm. Sci., **41**, pp. 1017–1027.
[13] Wang, C. C., Jeng, Y. R., Chien, J. J., and Chang, Y. J., 2004, "Friction Performance of Highly Viscous Fluid in Minichannels," Appl. Therm. Eng. **24**, pp. 2243–2250.
[14] Agostini, B., Watel, B., Bontemps, A., and Thonon, B., 2002, "Friction Factor and Heat Transfer Coefficient of R134a Liquid Flow in Mini-Channels," Appl. Therm. Eng. **22**. pp. 1821–1834.
[15] Downing, R. S., and Kojasoy, G., 2002, "Single and Two-Phase Pressure Drop Characteristics in Miniature Helical Channels," Exp. Therm. Fluid Sci., **26**, pp. 535–546.
[16] Downing, R. S., 1999, "Analytical and Experimental Study of Single and Two-Phase Cooling in Miniature Straight and Helical Channels," Ph.D. thesis, Department of Mechanical Engineering, University of Wisconsin-Milwaukee, Milwaukee, WI.
[17] Debray, F., Franc, J. P., Maitre, T., and Reynaud, S., 2001, "Measurement of Forced Convection Heat Transfer Coefficients in Minichannels," Mec. Ind., **2**, pp. 443–454.
[18] Reynaud, S., Debray, F., Franc, J. P., and Maitre, T., 2005, "Hydrodynamics and Heat Transfer in Two-Dimensional Minichannels," Int. J. Heat Mass Transfer, **48**, pp. 3197–3211.
[19] Liu, B. M., and Mui, Y., 2004, "Multi-Physics Simulation of a Microprocessor

Package Under Water Cooling," ASME J. Electron. Packag., **126**, pp. 384–389.
[20] Schmidt, R., 2003, "Challenges in Electronic Cooling—Opportunities for Enhanced-Thermal Management Techniques—Microprocessor Liquid Cooled Minichannel Heat Sink," *1st International Conference on Microchannels and Minichannels*, Rochester, NY, April 24–25.
[21] Yazawa, K., and Ishizuka, M., 2005, "A Study of Channel Optimization in Cooling Spreader on a Smaller and Transient Heat Source," *Proceedings of Fifth International Conference on Enhanced, Compact and Ultra-Compact Heat Exchangers: Science, Engineering and Technology*, Engineering Conferences International, Hoboken, NJ, September.
[22] Patankar, S. V., 1980, *Numerical Heat Transfer and Fluid Flow*, Hemisphere, New York.
[23] Tao, W. Q., 2001, *Numerical Heat Transfer*, 2nd ed., Xi'an Jiaotong University Press, Xi'an, China.
[24] Li, Z. Y., and Tao, W. Q., 2002, "A New Stability-Guaranteed Second-Order Difference Scheme," Numer. Heat Transfer, Part B, **42**(4), pp. 349–365.
[25] Yang, S. M., and Tao, W. Q. 1998, *Heat Transfer*, 3rd ed., Higher Education Press, Beijing, China.
[26] Rohsenow, W. M., and Hartnett, W. M., 1973, *Handbook of Heat Transfer*, McGraw-Hill, New York.
[27] Knight, R. W., Hall, D. J., Goodling, J. S., and Jaeger, R. C., 1992, "Heat Sink Optimization With Application to Microchannels," IEEE Trans. Compon., Hybrids, Manuf. Technol., **15**(5), pp. 832–842.
[28] Incropera, F. P., and DeWitt, D. P., 1996, *Introduction to Heat Transfer*, 3rd ed., John Wiley & Sons, New York.